Hindawi
Wireless Communications and Mobile Computing
Volume 2022, Article ID 5751316, 15 pages
https://doi.org/10.1155/2022/5751316

Research Article

Analysis of Multipath Fading and Doppler Effect with Multiple Reconfigurable Intelligent Surfaces in Mobile Wireless Networks

Guilu Wu,[1,2,3] **Fan Li**,[4] **and Huilin Jiang**[5]

[1]*State Key Laboratory of Millimeter Waves, Southeast University, Nanjing 211189, China*
[2]*National Mobile Communications Research Laboratory, Southeast University, Nanjing 211189, China*
[3]*School of Internet of Things Engineering, Jiangnan University, Wuxi 214122, China*
[4]*Institute of Forest Resource Information Techniques CAF, Beijing 100091, China*
[5]*School of Electronic Engineering, Nanjing Xiaozhuang University, Nanjing 211171, China*

Correspondence should be addressed to Huilin Jiang; huilin.jiang@njxzc.edu.cn

Received 31 July 2021; Accepted 10 December 2021; Published 17 January 2022

Academic Editor: Pan Tang

The multipath fading and Doppler effect are well-known phenomena affecting channel quality in mobile wireless communication systems. Within this context, the emergence of reconfigurable intelligence surfaces (RISs) brings a chance to achieve this goal. RISs as a potential solution are considered to be proposed in sixth generation (6G). The core idea of RISs is to change the channel characteristic from uncontrollable to controllable. This is reflected by some novel functionalities with wave absorption and abnormal reflection. In this paper, the multipath fading and Doppler effect are characterized by establishing a mathematical model from the perspective of reflectors and RISs in different mobile wireless communication processes. In addition, the solutions that improve the multipath fading and Doppler effect stemming from the movement of mobile transmitter are discussed by utilizing multiple RISs. A large number of experimental results demonstrate that the received signal strength abnormal fluctuations due to Doppler effect can be eliminated effectively by real-time control of RISs. Meanwhile, the multipath fading is also mitigated when all reflectors deployed are coated with RISs.

1. Introduction

Before the 6G mobile communication system, people are always exploring physical layer (PHY) technologies to improve system performance as fundamentally as possible, such as orthogonal frequency division multiplexing (OFDM) technology, massive multiple-input multiple-output (MIMO) technology, and millimeter wave (mmWave) communication [1]. The famous Nobel Prize winner George Bernard Shaw told us "Reasonable men adapt themselves to their environment; unreasonable men try to adapt their environment to themselves." As we all know, the wireless channel is the medium of information transmission. Traditional technologies cannot bring revolutionary ideas in improving PHY layer solutions, and they are at best a supplement to existing technologies. Hence, researchers have started research on revolutionary ideas from beyond 5G, especially on 6G technologies [2]. In this era, people expect new communication solutions could bring high spectral, energy efficiencies, reliability, and so on to satisfy the potential demands of various users and applications in future wireless communication systems, particular at the PHY.

Back to essence, the final goal of modern wireless communications is to build truly propagation channel and provide interference-free connection and high quality-of-service (QoS) to multiple users. The uncontrollable and random channel of wireless propagation environment is the culprit for the deterioration of communication performance, including multipath fading, severe attenuation, Doppler effect, and intersymbol interference. To overcome these difficulties, many modern PHY technologies are proposed in the next several decades [3]. However, the overall progress is still relatively slow as of the random behavior of wireless channel. In the past researches on wireless channel, researchers often

assume it is an uncontrollable entity and brings a negative effect on the performance of wireless communication system. Fortunately, the progress of electromagnetic (EM) material brings the dawn of victory. This technology facilitates the emergence of reconfigurable intelligent surfaces (RISs), which are manmade surfaces composed of EM material. RISs have unique functions on wave absorption, anomalous reflection, phase modification, and wave regulation for EM wave transmission. In addition, the structure of communication system is simplified when RISs can replace the complex baseband processing and radiofrequency (RF) transceiver operations [4]. The novelty paradigm of intelligent communication environments is exploited on the communication efficiency and the QoS. In short, the major contributions in this paper can be summarized as follows:

(1) The novel and specific mathematical model is proposed to analyze the received signal in mobile communication environments facing multipath fading and Doppler effect. Specifically, the amplitude and phase are considered to represent signal information in process of exploring the new paradigm

(2) The analysis of multiple reflectors and RISs-assisted communication cases are discussed on the proposed mathematical model when the transmitter is moving. For these cases, the directed transmission signal and multiple signals stemming from multiple reflectors or RISs are included in mobile communication environments

(3) By comparison, the corresponding model is also proposed and discussed to analyze the received signal when the directed link between the transmitter and receiver is blocked in the multiple reflectors and RISs-assisted systems

(4) The results on the multipath fading and Doppler effect are verified in simulation environments for reflectors-/RISs-assisted communication environments. And the specific analysis are provided in the received signal strength when multiple reflectors are coated with RISs

The rest of this paper is organized as follows: Section 2 describes the related works that the PHY layer technologies solve the high spectral efficiency, energy efficiency, transmission reliability, and so on in 6G wireless communication systems. Then, the system scenario and the analysis model of received signal in the case of multiple reflectors are designed to depict the multipath fading and Doppler effect in Section 3. Meanwhile, the solution is also give out by using the real-time tuneable RISs. In Section 4, we provide analysis of eliminating Doppler effect through multiple RISs when the directed transmission link is blocked between transmitter and receiver. In Section 5, simulation results display the performance analysis of the received signal on complex envelope magnitude. The specific effects on signals due to the number of RISs are discussed and analyzed specifically. Finally, Section 6 concludes this paper and gives the future research work.

2. Related Works

There are many modern PHY technologies, including modulation technology, coding, nonorthogonal multiple access (NOMA) technology, cooperation communication, beamforming, and smart antenna array to overcome wireless propagation problems, such as deep fading, propagation attenuation, and Doppler effect, in the presence of harsh communication environments. These problems lead to the slow progress from 1G to 5G networks. Meanwhile, they will bring challenges in the beyond 5G and 6G networks. In essence, the random and uncontrollable propagation environment degrades the received signal quality and communication QoS [5]. In traditional wireless networks, researchers make great efforts on transmitter and received ends to explore enhancing communication efficiency and QoS by setting a negative factor term in the communication process [6, 7].

Recently, the emergence of RISs reshapes the random and uncontrollable communication environments to improve the performance of mobile wireless networks. Meanwhile, RISs provide a new paradigm in 6G communication, denoted as RISs-assisted wireless networks. An unreasonable communication entity and distinguishing feature, including passive units, reconfigurable mechanism, and simple deployment, attract the attention of researchers in RISs-assisted wireless networks [8]. The main objective of this paper is to challenge signal quality and QoS by exploiting this intelligent communication networks. To achieve signal quality and QoS, rich channel information is a really good way in communication environments. [9, 10] and [11] propose novel physical modulation technologies to exploit reconfigurable antennas or scattering wireless environments. Furthermore, the change of wireless communication environments could improve communication quality by adopting reflector and scatter such as intelligent walls [12], programmable metasurfaces [13], reconfigurable intelligent antenna array [14], and intelligent metasurfaces [15]. These works affect complexity, power consumption, and performance analysis of wireless networks.

The concept of RISs as a controllable device enhance aforementioned function as of its controllability on propagation environments. Many works focus on link transmission metric [16–20], channel estimation [21–24], PHY security [25–27], and practical applications [28–30] to analyze performance of RISs-assisted systems. Specifically, [16] optimizes transmission power and reflection coefficient to achieve sum-rate maximization when each mobile user has QoS guarantee. Considering link budget guarantee of a user in downlink communication, [17] proposes an energy-efficient scheme by joint optimization transmission power allocation and RIS phase shift. Combined with transmitter and receiver, [18] optimizes beamforming vector, combining vector, and phase shifts at transmitter to maximize SNR at the receiver. When interference is introduced to user, the transmit power is allocated in [19] by joint active and passive beamforming to improve the performance of RISs-assisted wireless networks. When facing transmission distance, the quantitative analysis with wireless coverage and

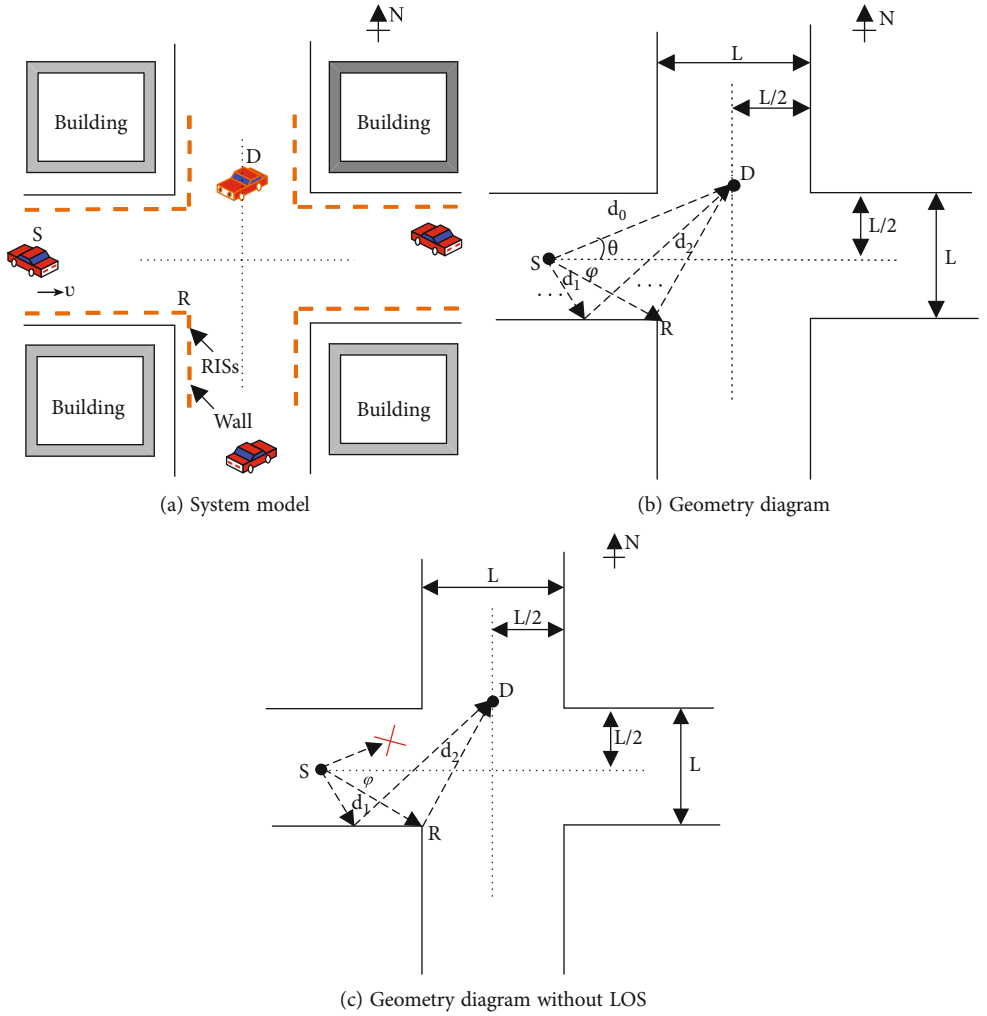

(a) System model

(b) Geometry diagram

(c) Geometry diagram without LOS

Figure 1: A simple multiple reflectors-/RISs-assisted mobile wireless communication systems.

SNR gain is presented in [20] for RISs-assisted system. These works require to acquire accurate channel information in application. Two efficient channel estimation schemes are proposed in [21] in RISs-assisted multiusers communication systems. Then, [22] proposes a pilot-assisted method to solve channel estimation problem in receiver. To reduce training overhead, [23] exploits the channel information by using the inherent sparsity and [24] designs a low complexity channel estimation method to attain the separate channel state information in MIMO system. For PHY technologies, security is also an important issue, beside RISs-assisted networks. In [25], RISs as a backscatter device to process scatter jamming signal in secure transmission when the transmitter is radiofrequency source. And [26] proposes an effective conjugate gradient algorithm to enhance PHY security by joint optimization the active and passive beamforming in downlink communication. For adopting channel state information, RIS units are investigated in [27] to improve the secret key capacity in RISs-assisted secret key generation. The performance analysis of RISs-assisted system on physical technologies has been extensively discussed in ideal conditions in prior works. Considering practical applications, [28] studies phase shift model by capturing the phase-dependent amplitude variation in RISs-assisted system. Furthermore, [29, 30] study minimization power problem in downlink communication and channel aligning on cell-edge users in communication systems.

Table 1: Summary of system parameters.

Parameters	Value
Initial distance (s)	[800,600,400,200]m
Carrier frequency (f_c)	3×10^9 m/s
Speed	10 m/s
Number of reflectors	[1–4]

The existing works have brought us momentum on PHY technologies in RISs-assisted systems. In this paper, we focus on the multipath fading and Doppler effect in RISs-assisted wireless networks. They are ubiquitous in wireless networks and have huge impact on network performance. Hence, the in-depth discussion on multipath fading and Doppler effect mitigation is important in RISs-assisted systems.

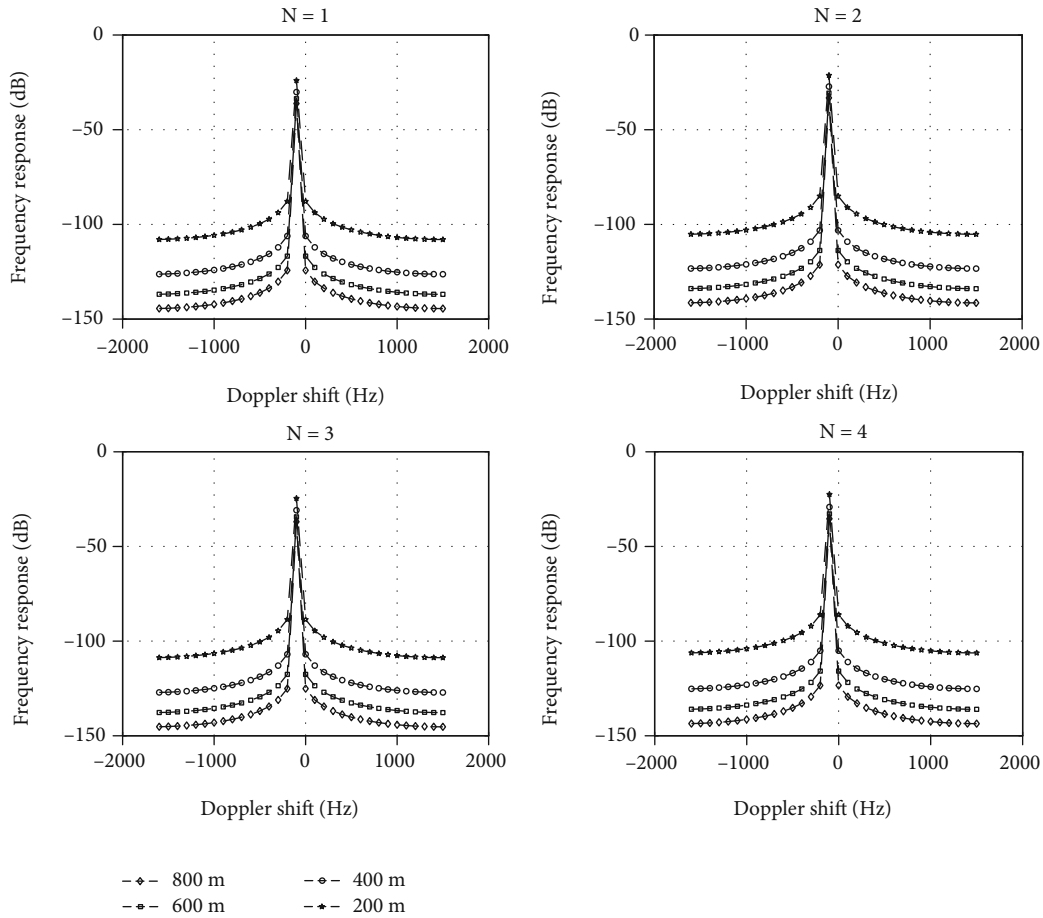

Figure 2: Doppler shift of the received signal for varying number of multiple reflectors at different initial distances. Geometry diagram of vehicle-to-vehicle communication for two reflectors without LOS path.

3. Scenario Description and System Model

3.1. Scenario Description. A communication transmission between vehicle S and vehicle D in ITS is considered in Figure 1(a). The vehicle S moves along the street from west to east at speed v in urban. A signal from the vehicle S is transmitted to the vehicle D, which is waiting for red traffic lights in crossroads. The transmission paths include a directing link (line of sight, LOS) and multiple reflecting links (nonline of sight (NLOS)). The corresponding geometric plan is plotted in Figure 1(b). We assume the vehicle S departure from location $(-s, 0)$, $s \geq L/2$ and the vehicle D stays at position $(0, L/2)$ (for convenience of description and calculation, the location of the vehicle S and D are denoted specially in coordinate system. However, this method in this paper is not limited to a specific location.). Hence, the distance of LOS path between the vehicle S and the vehicle D is

$$d_0 = \sqrt{s^2 + \left(\frac{L}{2}\right)^2}. \tag{1}$$

The N reflectors are evenly and linearly deployed on the each side of wall, and the distance between adjacent reflector is defined as w. In practice, the deployment cost of reflectors is a factor to consider, especially for RISs. Without loss of generality, a short distance near the intersection can be applied to deploy reflectors/RISs in Figure 1(a). Based on geometric relations from Figure 1(b), we assume the reflector deployed near the corner of the traffic intersection is denoted as 0. Hence, the position of the ith reflector is $(-(iw + L/2), -L/2)$, $i = 0, 1, \cdots, N$. Then, the distance of NLOS path based on ith reflection point can be given by

$$\begin{cases} d_1 = \sqrt{\left[s - \left(iw + \dfrac{L}{2}\right)\right]^2 + \left(\dfrac{L}{2}\right)^2}, \\ d_2 = \sqrt{\left(iw + \dfrac{L}{2}\right)^2 + L^2}. \end{cases} \tag{2}$$

In addition, the angles formed, respectively, by the transmission direction and the horizontal direction, θ and φ, from the vehicle S signal for the LOS link and the NLOS link are written by

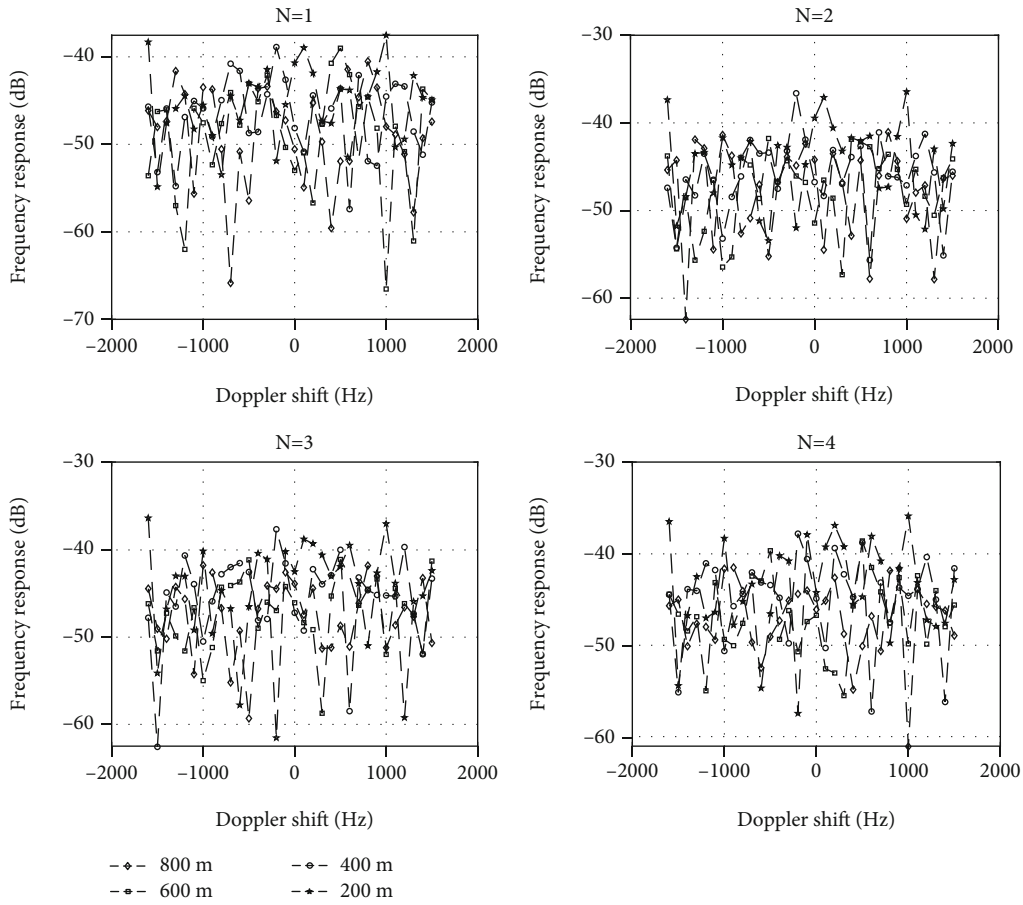

Figure 3: Doppler shift of the received signal for varying number of multiple reflectors when vehicle S moves from different distances. Doppler shift of the received signal for varying number of multiple reflectors at different initial distances.

$$\begin{cases} \theta = \arcsin^{-1}\left(\dfrac{L/2}{d_0}\right), \\ \varphi = \arcsin^{-1}\left(\dfrac{L/2}{d_1}\right). \end{cases} \tag{3}$$

From the Figure 1(b), the location of the vehicle S changes with its movement at time t. Therefore, the distance with Equations (1) and (2) can be rewritten by

$$d(t) = d - v't, \tag{4}$$

where d represents the initial value of distance and v' is the speed in the direction of signal transmission. Meanwhile, when the reflection point i is different, the θ and φ change accordingly over time t.

Apparently, the Doppler shift occurs due to movement during the signal transmission of the vehicle. When the carrier frequency of signal is f_c, the Doppler shifts in different directions can be given by

$$\begin{cases} f_{d_i} = \dfrac{v}{\lambda_c}\cos\theta_i = f_c\dfrac{v}{c}\cos\theta_i, \\ f_{r_i} = \dfrac{v}{\lambda_c}\cos\varphi_i = f_c\dfrac{v}{c}\cos\varphi_i, \end{cases} \tag{5}$$

where c is the speed of light.

3.2. Mathematical Model of Transmission Signal. The transmission signal is from the moving vehicle S, and it is an unmodulated RF carrier signal, denoted as $s(t)$. Hence, the initial expression of this signal can be written by

$$s(t) = A\cos\left(2\pi f_c t + \Psi_0\right), \tag{6}$$

where A is amplitude of $s(t)$ and we define $A = 1$ for the convenience of analysis, and f_c is the carrier frequency of transmission signal, and Ψ_0 is the initial phase.

Generally, the amplitude and phase include all information of the transmission signal. Hence, the Equation (6) can be represented by a simple complex baseband form when it passes through the low-pass filter as follows:

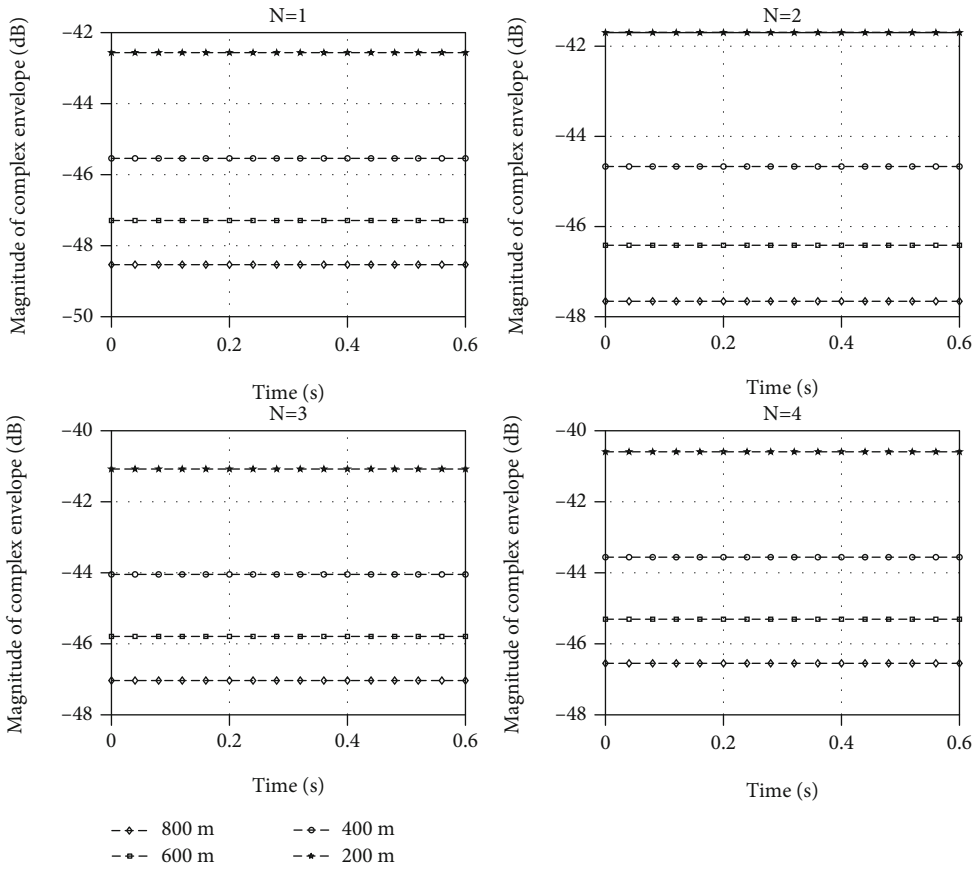

Figure 4: Doppler shift of the received signal for varying number of multiple reflectors at different initial distances. Doppler shift of the received signal for varying number of multiple reflectors when vehicle S moves from different distances.

$$s(t) = \exp(j\Psi_0). \tag{7}$$

3.3. LOS and Multiple NLOS Transmission without RISs. From Figure 1(b), the vehicle D can receive multipath signals, including LOS ($S \longrightarrow D$) and multiple NLOS ($S \longrightarrow R_i \longrightarrow D$) signals. We assume that all incident wave can be reflected and received in received terminal as of reasonable angle of reflection. Hence, the received combined signal is given by

$$r(t) = r_0(t) + \sum_{i=1}^{i=N} r_i(t). \tag{8}$$

where $r_0(t)$ and $r_i(t)$ represent LOS link signal and the i th NLOS link signal, respectively.

Due to the vehicle S movement, the transmission signal will encounter multipath fading and Doppler spectrum shift in communication. We assume the LOS signal and NLOS signal have almost constant amplitudes when they have rapidly varying phase terms. We focus on the multipath fading and Doppler spectrum shift at the receiver by observing complex envelope of signal [31, 32]. It is given by

$$r_c(t) = \frac{\lambda_c}{4\pi}\left(\frac{e^{-jk_c d_0(t)}}{d_0(t)} + \sum_{i=1}^{N}\sigma_i(t)\frac{e^{-jk_c\left(d_{1_i}(t)+d_{2_i}(t)\right)}}{d_{1_i}(t)+d_{2_i}(t)}\right), \tag{9}$$

where k_c is the transmission coefficient, denoted as $k_c = 2\pi/\lambda_c$ and σ_i is the reflection coefficient of the ith reflection link through reflector.

3.4. Multipath Fading and Doppler Shift for Communication. Normally, we assume N reflectors are deployed on one side of the wall and the reflection coefficient is one. The vehicle D receives multipath transmission signals. We focus into a vary short time interval with Figure 1(a). Hence, the combined signal in the received D based on Equation (9) can be given by

$$\begin{aligned} r_c(t) &= \frac{\lambda_c}{4\pi}\left(\frac{e^{-jk_c d_0(t)}}{d_0(t)} + \sum_{i=1}^{N}\frac{e^{-jk_c\left(d_{1_i}(t)+d_{2_i}(t)\right)}}{d_{1_i}(t)+d_{2_i}(t)}\right) \\ &= \frac{\lambda_c}{4\pi}\left(\frac{e^{-j(2\pi/\lambda_c)(d_0-v\cos\theta_i t)}}{d_0} + \sum_{i=1}^{N}\frac{e^{-j(2\pi/\lambda_c)\left(\left(d_{1_i}-v\cos\varphi_i t\right)+d_{2_i}\right)}}{d_{1_i}+d_{2_i}}\right) \\ &= \frac{\lambda_c}{4\pi}\left(\frac{e^{-j\Phi_0+j2\pi f_d\cos\theta_i t}}{d_0} + \sum_{i=1}^{N}\frac{e^{-j\left(\Phi_{1_i}+\Phi_{2_i}\right)+j2\pi f_r\cos\varphi_i t}}{d_{1_i}+d_{2_i}}\right), \end{aligned} \tag{10}$$

where $\Phi_0 = (2\pi/\lambda_c)d_0$, $\Phi_{1_i} = (2\pi/\lambda_c)d_{1_i}$, and $\Phi_{2_i} = (2\pi/\lambda_c)d_{2_i}$.

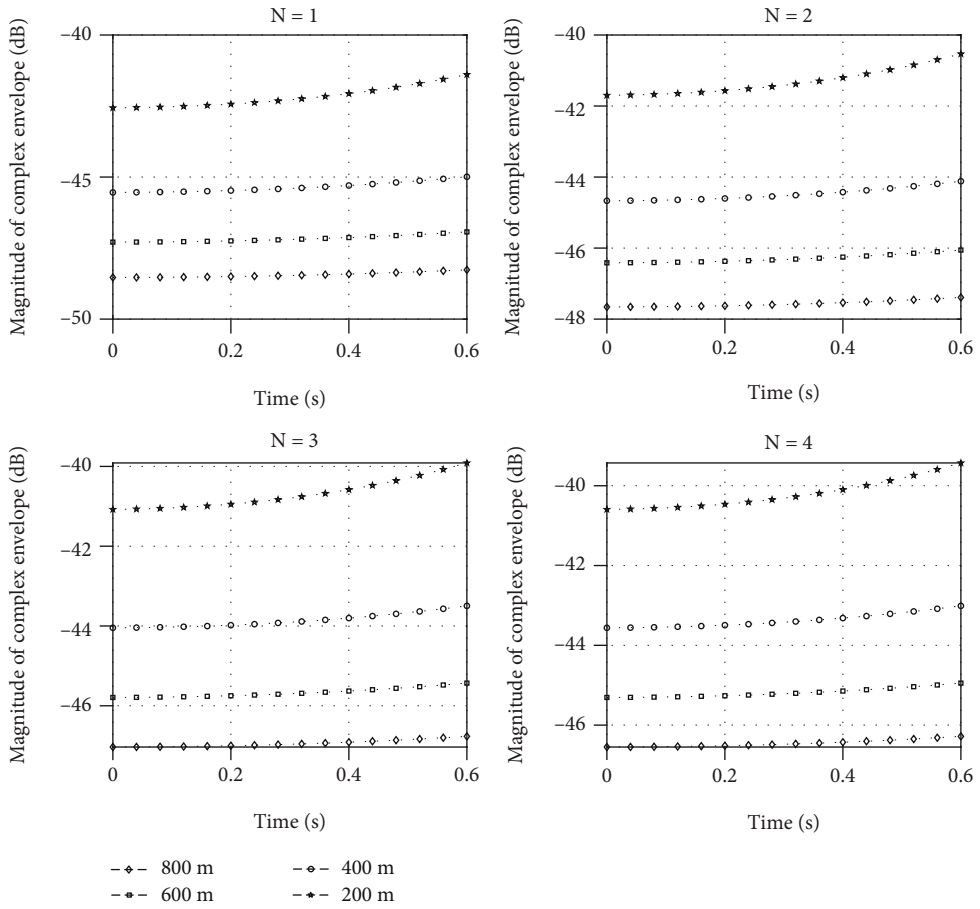

Figure 5: The magnitude of received signal in the presence of multiple reflectors when vehicle S moves from different initial distances. Doppler shift of the received signal for varying number of multiple reflectors at different initial distances.

Apparently, the constant terms Φ_0 and $\Phi_{1_i} + \Phi_{2_i}$ in Equation (10) can be dropped when they are integer multiples of 2π. Hence, the properties of complex exponentials can be adopted to obtain the magnitude of this complex envelope. It is given by

$$|r(t)| = \frac{\lambda_c}{4\pi}\left(\frac{1}{d_0^2} + \sum_{i=1}^{N}\frac{1}{\left(d_{1_i} + d_{2_i}\right)^2} + X\left(d_0, d_{1_i} + d_{2_i}, f_{d_i}\cos\theta_i, f_{r_i}\cos\varphi_i\right)\right)^{1/2}. \quad (11)$$

In order to get the Equation (11), Equation (10) operates polynomial perfect square expansion. The total items is $\binom{N+2}{2}$, where $N+1$ items are their respective square item, and X items are product between any two items that are not repeated for $N+1$ items mentioned before and two times the product of $\cos 2\pi f_{d_i}\cos\theta_i t$ and $\cos 2\pi f_{r_i}\cos\varphi_i t$ is corresponding coefficient for each item (in this paper, f_{d_i} and f_{r_i} are different for different transmission reflection paths. We assume $f_{d_i}\cos\theta_i$ and $f_{r_i}\cos\varphi_i$ are basically unchanged when θ and φ change slowly). To sum up, X includes $((N+2)/(2\cdot N!)) - N - 1$ items.

3.5. Eliminating Multipath Fading through RISs. The different distances of multipath transmission cause difference in the arrival time and phases of the reflected waves. The superposition of multiple signals with different phases at the receiving end makes the amplitude of the received signal change sharply to produce multipath fading. When the reflector is RISs, the direction of the reflected beam can be adjusted arbitrarily through controller (i.e., FPGA). In this paper, we assume the reflection coefficient of an RIS is a time-varying and unit-gain. Hence,

$$\sigma(t) = e^{j\psi(t)}, \quad (12)$$

where ψ is the phase of RIS.

For multiple RISs case, the vehicle D receives multipath transmission signals. Hence, the combined signal in the received D based on Equations (9) and (12) can be rewritten by

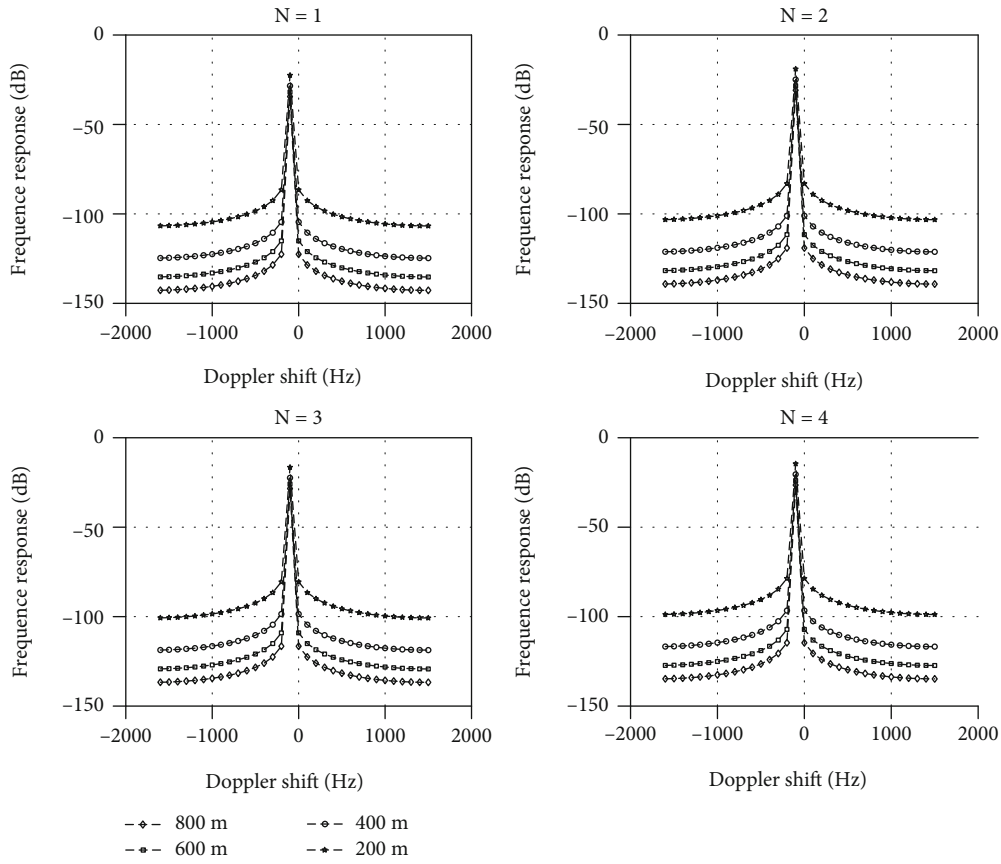

Figure 6: Doppler shift of the received signal for varying number of multiple RISs at different initial distances. The magnitude of received signal in the presence of multiple reflectors when the vehicle S moves from different initial distances.

$$r_c(t) = \frac{\lambda_c}{4\pi}\left(\frac{e^{-jk_c d_0(t)}}{d_0(t)} + \sum_{i=1}^{N} e^{j\psi_i(t)}\frac{e^{-jk_c\left(d_{1_i}(t)+d_{2_i}(t)\right)}}{d_{1_i}(t)+d_{2_i}(t)}\right) = \frac{\lambda_c}{4\pi}\left(\frac{e^{-j(2\pi/\lambda_c)(d_0 - v\cos\theta_i t)}}{d_0} + \sum_{i=1}^{N} e^{j\psi_i(t)}\frac{e^{-j(2\pi/\lambda_c)\left(\left(d_{1_i} - v\cos\varphi_i t\right)+d_{2_i}\right)}}{d_{1_i}+d_{2_i}}\right). \quad (13)$$

The received complex envelop for Equation (13) can be rewritten by

$$r_c(t) = \frac{\lambda_c}{4\pi}\left(\frac{e^{j2\pi f_{d_i}\cos\theta_i t}}{d_0} + \sum_{i=1}^{N}\frac{e^{j2\pi f_{r_i}\cos\varphi_i t + j\psi_i(t)}}{d_{1_i}+d_{2_i}}\right). \quad (14)$$

When the magnitude of $r(t)$ is maximized, the phases of direct and multiple reflected signals are aligned, that is, by adjusting. For the sake of simplicity and without loss of generality, the phases adjustment of multiple RISs under different transmission links are handled as the phases accumulation of multiple RISs. Hence, the magnitude of $r_c(t)$ is maximized when the jointed phase of RISs is

$$\sum_{i=1}^{N}\psi_i(t) = 2\pi\left(\sum_{i=1}^{N} f_{r_i}\cos\varphi_i - f_{d_i}\cos\theta_i\right)t \mod 2\pi, \quad (15)$$

and then, the complex envelope of the Equation (14) is computed as

$$r_c(t) = \frac{\lambda_c e^{j2\pi f_{d_i}\cos\theta_i t}}{4\pi}\left(\frac{1}{d_0} + \sum_{i=1}^{N}\frac{1}{d_{1_i}+d_{2_i}}\right). \quad (16)$$

During our observation interval, the maximized magnitude of Equation (16) can be expressed as

$$|r_c(t)|_{\max} = \frac{\lambda_c}{4\pi}\left(\frac{1}{d_0} + \sum_{i=1}^{N}\frac{1}{d_{1_i}+d_{2_i}}\right). \quad (17)$$

The result indicates that the received signal strength increases when the components of multiple path signals are superimposed at the receiving end. That is because the phases of multiple path signals are aligned based on Equation (15).

3.6. Increasing Multipath Fading and Doppler Shift for RISs-Assisted Communication. In Section 3.5, the maximization of the received signal strength by RIS-assisted communication is the major content on discussion. Unfortunately, the received signal strength might be deterioration when the Doppler spread increases as of an unintended mobile user. And the maximum magnitude in Equation (17) can be

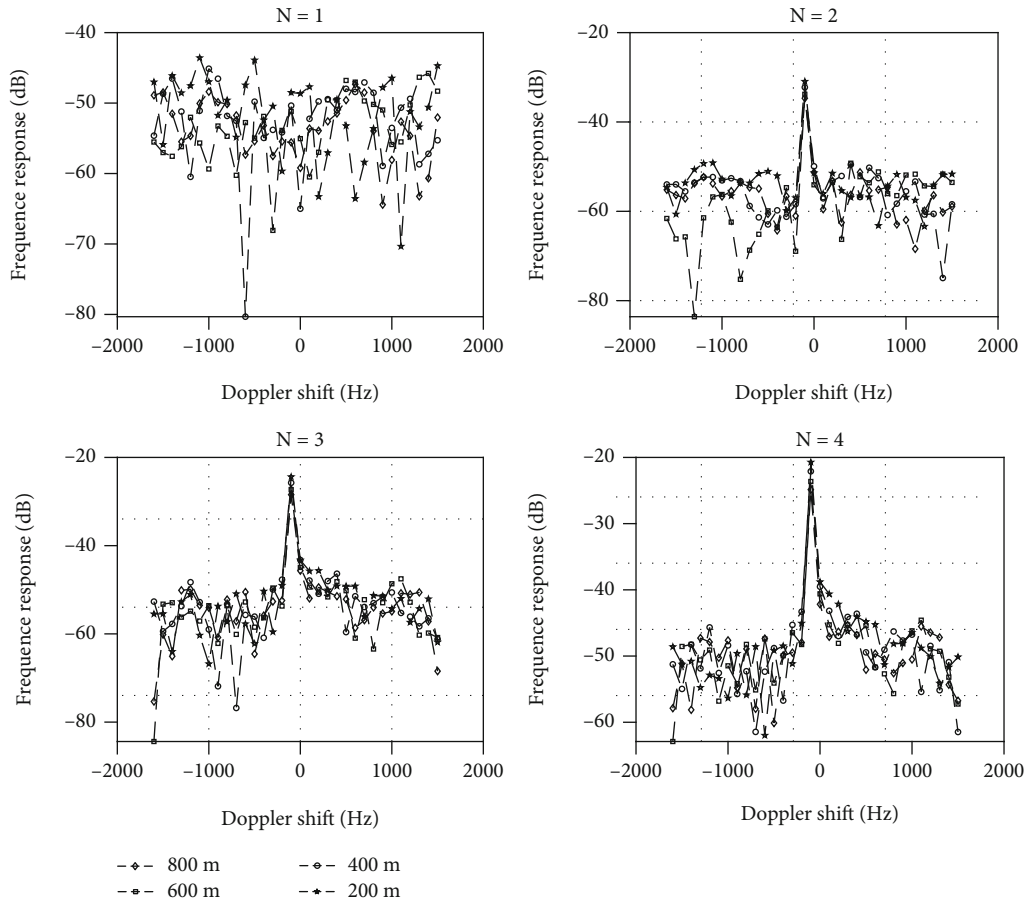

Figure 7: Doppler shift of the received signal for varying number of multiple RISs when vehicle S moves from different distances. Doppler shift of the received signal for varying number of multiple RISs at different initial distances.

achieved when the received two signals are in same phase from Equation (13). Similarly, the jointed phase of RISs in Equation (14) is following

$$\sum_{i=1}^{N}\varphi_i(t) = \left[2\pi\left(\sum_{i=1}^{N} f_{r_i}\cos\varphi_i - f_{d_i}\cos\theta_i\right)t + \pi\right] \mod 2\pi. \tag{18}$$

At this case, the received signal strength decreases when the components of multiple path signals are superimposed at the receiving end. By now, the arriving signals are completely out-of-phase and the complex envelope magnitude becomes minimize value, which is

$$|r_c(t)|_{\min} = \frac{\lambda_c}{4\pi}\left(\frac{1}{d_0} - \sum_{i=1}^{N}\frac{1}{d_{1_i} + d_{2_i}}\right). \tag{19}$$

From Equation (19), the result shows the degradation in the received combined signal strength is more obvious for approximate relationship, d_0 and $\sum_{i=1}^{N}(d_{1_i} + d_{2_i})$. However, this relationship prevents drastic changes in the complex envelope of Equation (17).

4. Eliminating Doppler Shift through RISs

When the LOS between the vehicle S and the vehicle D is blocked, the NLOS link is built through multiple RISs as shown in Figure 1(c). The assumptions of Section 3.1 are also applied in this section. The Doppler shift on the received signal is mainly investigated as follows.

4.1. Without Multiple RISs-Assisted NLOS transmission. From Section 3.4 and NLOS communication case, the received signals on the vehicle D are from multiple reflectors-assisted when the reflection coefficient of reflector is one. The result can be expressed as

$$r_c(t) = \frac{\lambda_c}{4\pi}\sum_{i=1}^{N}\frac{e^{-j(2\pi/\lambda_c)\left(d_{1_i}(t)+d_{2_i}(t)\right)}}{d_{1_i}(t) + d_{2_i}(t)}, \tag{20}$$

It can be seen from Figure 1(c) that $d_{2_i}(t)$ has nothing to do with the vehicle S speed (the distance between reflection point and received end is fixed when the reflection point and received end are fixed in this paper). And $d_{1_i}(t) = d_{1_i} - v\cos\varphi_i t$ has relationship with the vehicle S speed v. Similarly, we ignore the constant term and observe a short travel distance. Then, Equation (20) is rewritten by

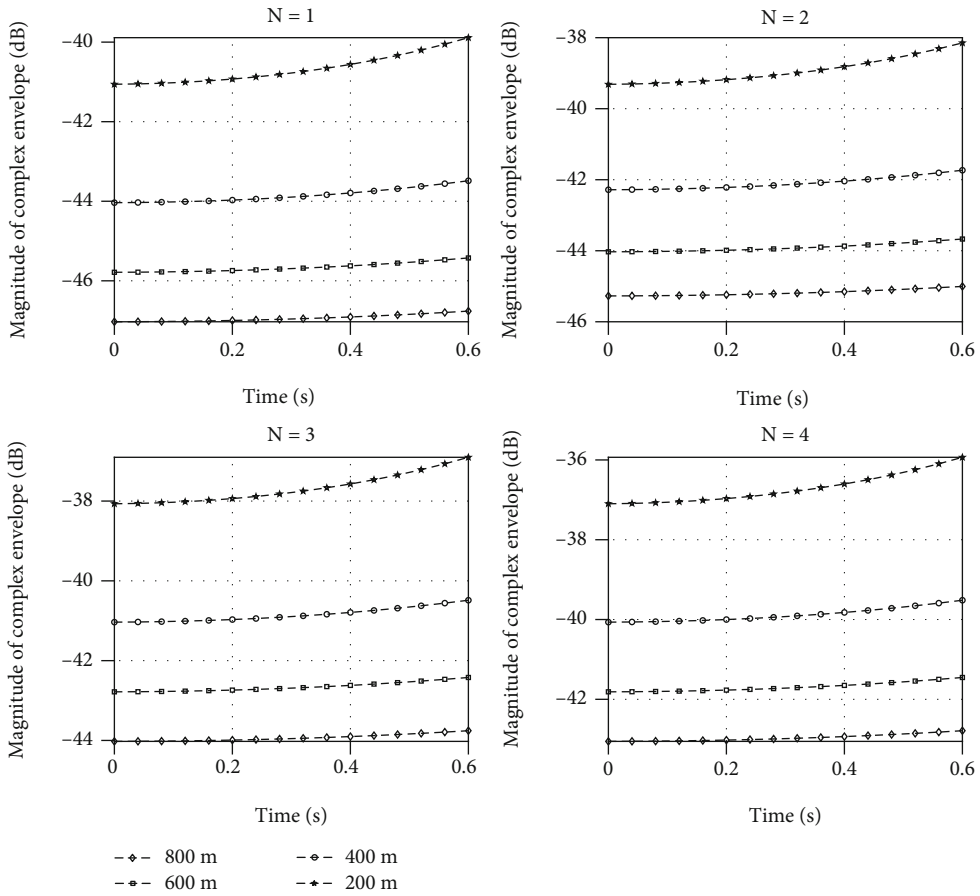

Figure 8: The maximized magnitude of received signals at vehicle D when the initial distance is fixed in RISs-assisted wireless communication systems. Doppler shift of the received signal for varying number of multiple RISs when vehicle S moves from different distances.

$$r_c(t) = \frac{\lambda_c}{4\pi} \sum_{i=1}^{N} \frac{e^{j2\pi f_{r_i} \cos \varphi_i t}}{d_{1_i}(t) + d_{2_i}(t)}. \tag{21}$$

Apparently, Equation (21) shows that the combined signal received has a Doppler frequency shift of $f_{r_i} \cos \varphi_i$ Hz on the ith reflection point due to the movement of the vehicle S. From Equation (21), although multiple reflections occur without a LOS signal, the combined signal received magnitude at the vehicle D does not undergo a fade pattern when these reflections own consistent operation during a short time interval. The specific magnitude of the Equation (21) is given by

$$|r_c(t)| = \frac{\lambda_c}{4\pi} \sum_{i=1}^{N} \frac{1}{d_{1_i}(t) + d_{2_i}(t)}. \tag{22}$$

4.2. Multiple RISs-Assisted NLOS transmission. There are multiple RISs that are able to provide adjustable phase shifts, denoted as $\sigma_i(t) = e^{j\psi_i(t)}$ and NLOS communication links without a LOS signal as shown in Figure 1(c). Similar to Section 3.5, the combined signal received at the vehicle D can be expressed as

$$r_c(t) = \frac{\lambda_c}{4\pi} \sum_{i=1}^{N} \frac{e^{j\left(2\pi f_{r_i} \cos \varphi_i t + \psi_i(t)\right)}}{d_{1_i}(t) + d_{2_i}(t)}. \tag{23}$$

Equation (23) indicates that the magnitude of the combined signal received at the vehicle D can obtain the same value as Equation (22) in case of $\psi_i(t) = -2\pi f_{r_i} \cos \varphi_i t \mod 2\pi$. The corresponding phase $\psi_i(t)$ can be reached by adjusting multiple RIS reflection phases.

5. Simulation Results

5.1. Simulation Setup. Given the system model adopted in Section 3.1 and the nature of mobile wireless environments, it is critical to analyze the performance of the received signal due to multipath fading and Doppler effect in propagation environments. This motivates using the received signal by reflectors to capture the dependence on the key network parameters such as the system geometry, the transmitter location, the number of reflectors or RISs, etc. To do that, we setup scenario and parameters, to generate the communication systems. The multiple reflectors are deployed on the wall that reflects the signal received from vehicle S to vehicle D. Vehicle D is assumed to be fixed while vehicle S moves

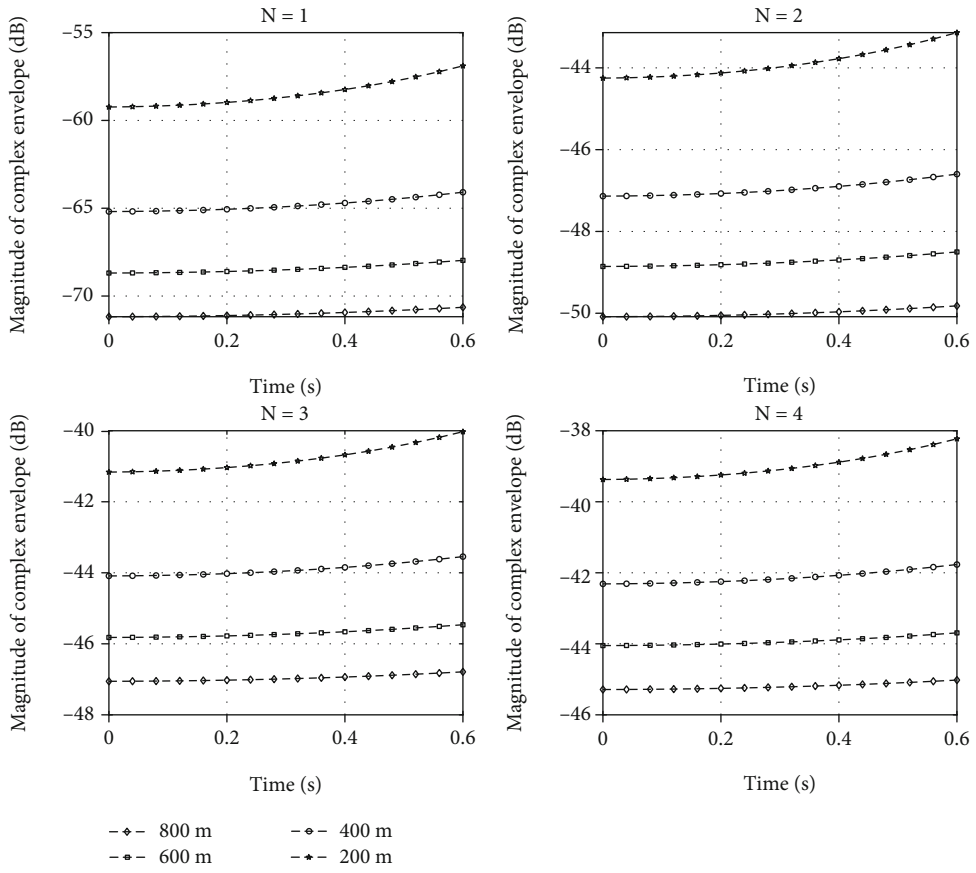

FIGURE 9: The minimize magnitude of received signals at the vehicle D when the initial distance is fixed in RISs-assisted wireless communication systems. The maximized magnitude of received signals at vehicle D when the initial distance is fixed in RISs-assisted wireless communication systems. The maximized magnitude of received signals at vehicle D when the initial distance is fixed in RISs-assisted wireless communication systems.

from west to east at any initial position as illustrated in Figure 1(a). Some critical parameters are given out in Table 1. The specific analysis on reflectors and RISs cases will be carried out as follows.

5.2. Analysis on Reflector Case. Obviously, the received signal at the vehicle D include the LOS signal ($S \longrightarrow D$) and multiple NLOS signals ($S \longrightarrow R \longrightarrow D$). The destructive and constructive interference is caused when these signals are combined at vehicle D. From Equation (11), the received signal strength fluctuates with a frequency known from X, which is affected by the path loss. Hence, the fade phenomenon of the received signal envelop is observed by this fluctuation. The variation of frequency response is shown in Figure 2 with different initial distances when different numbers of reflectors are deployed at sidewalls. On the whole, the frequency response gradually increases up to the top point and then its value gradually decreases for different initial distance. And from Equation (10), the corresponding Doppler shift which deviates from the center of carrier frequency f_c can be verified by the received signal in Figure 2. With increasing distance from 200 m to 800 m, the frequency response caused by the driving of the transmitter is weakened. The corresponding result variation is from about 39 % to about 36% when $N = 1$ to $N = 4$. Hence, the spacing between the curves at the two ends is reduced for different number of reflectors. In this process, Figure 3 displays the variation of frequency response at different numbers of reflectors when vehicle S moves along street from different initial distances.

From the perspective of receiver, the magnitude of complex envelop with respect to time at different initial distance are displayed in Figures 4 and 5 for different numbers of reflectors. The results are corresponding to fixed initial distance and varying distance in real time, respectively. Specifically, the magnitude of complex envelope appears slow climb with time cost for different initial distance and number of reflectors in Figures 4 and 5. It is noted that the magnitude of complex envelope has significant rise with increasing of reflectors. In Figure 4, the magnitude of complex envelope is from about -42.5 dB to -48.6 dB when the initial distance changes from 200 m to 800 m for $N = 1$. This result has changed from about -40.5 dB to -46.7 dB for $N = 4$. Similarly, the magnitude of complex envelope climbs from about -42.5 dB to -41.5 dB with increasing time for $N = 1$ when the initial distance is 200 m from Figure 5. And this result is about -48.6 dB to -48.1 dB in initial distance 800 m. When the number of reflectors is $N = 4$, the corresponding result changes from about -40.5 dB to -39.5 dB with increasing time for 200 m. And this result is from about

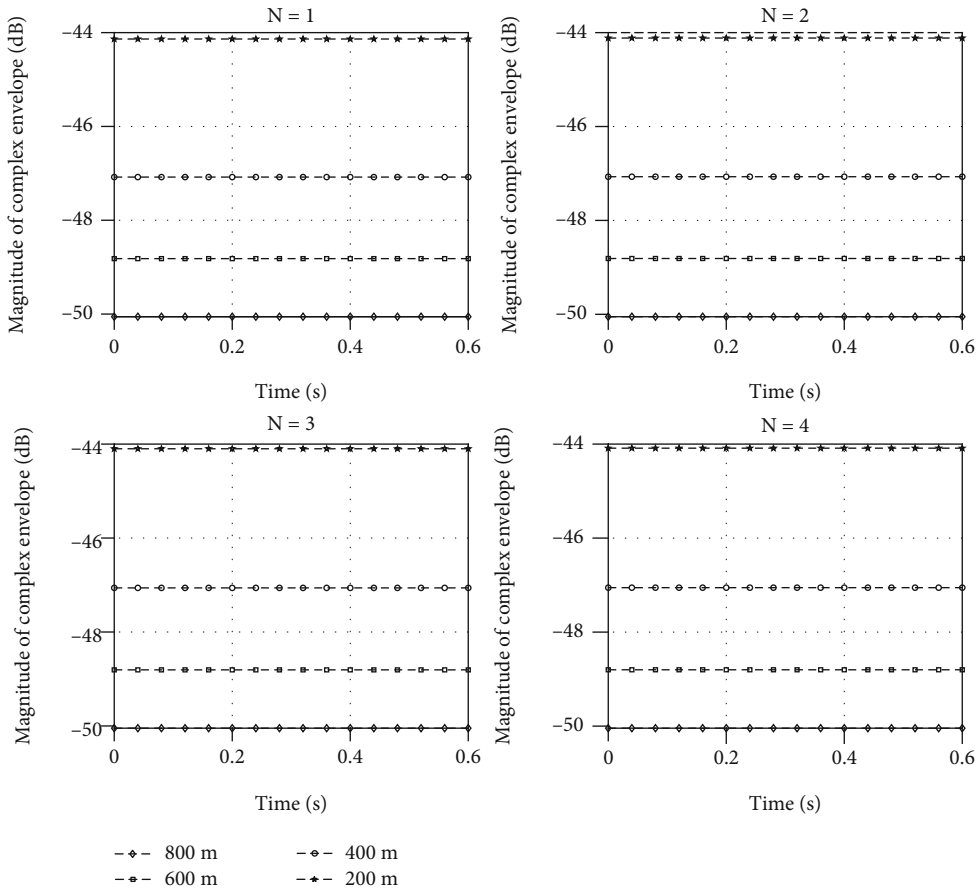

Figure 10: The magnitude of the received signal on vehicle D at case of different initial distance for Equation (22). The minimize magnitude of received signals at vehicle D when the initial distance is fixed in RISs-assisted wireless communication systems.

-46.5 dB to -46.1 dB for 800 m. Compared with Figures 2 and 3, the magnitude of complex envelope has significant improvement in Figure 5 when vehicle S moves along street in the communication process.

5.3. Analysis on RIS Case. The analysis of received signal on vehicle D is discussed when the transmission signal is reflected through reflectors. When all reflectors are coated with RISs, the received signal envelope is derived from Equation (16). It shows that the received signal strength can be eliminated appropriately as diversity gain produced by multipath transmission. Meanwhile, the corresponding multipath fading and Doppler shift can be mitigated through real-time tunable RISs. The simulation results are plotted in Figures 6 and 7. In Figure 6, we depict the frequency response of received signal at vehicle D when vehicle S locates different initial distances. With vehicle S moves along street, the change in frequency response is illustrated in Figure 7. Compared with Figures 2 and 3, the frequency response values increased are demonstrated on RISs-assisted networks by Figures 6 and 7.

Apparently, the frequency response takes RISs for the received signal to improves more. At different initial distances for 200 m, 400 m, 600 m, and 800 m, the variation in the frequency response is relatively small when $N = 1$. However, the frequency response increases by about 2% when the initial distance is 200 m for $N = 2$ and this case will increase to about 6% for $N = 4$. In addition, the RIS technology can play a greater advantage for long initial distances. Observing Figures 2 and 6, the frequency response increases by about 1% when the initial distance is 800 m for $N = 2$ and its gain will reach to about 8% for $N = 8$. Furthermore, the results also prove that the multipath fading is alleviated in this process with increasing distance.

The maximized magnitude of the complex envelope of received signal on vehicle D for the case of movement of vehicle S is displayed in Figure 8. For different initial distances of vehicle S, the $2\pi f_{d_i} \cos \theta_i t$ is zero under different numbers of RISs. In other words, the phases with LOS signal and NLOS signal are aligned assisted by RISs when multipath signals are combined at vehicle D. Conversely, the minimize magnitude of the complex envelope of received signal is also plotted in Figure 9. The results illustrate the phases with LOS signal and NLOS signal have inverted phase when they are combined at vehicle D. It can be seen that RISs bring an intuitive impact on the received signal in RISs-assisted communication environments after it acts on the transmission signal.

Observing the magnitude gain of received signals from RISs, when vehicle S moves along street from the initial distance 200 m, the maximized magnitude of received signals

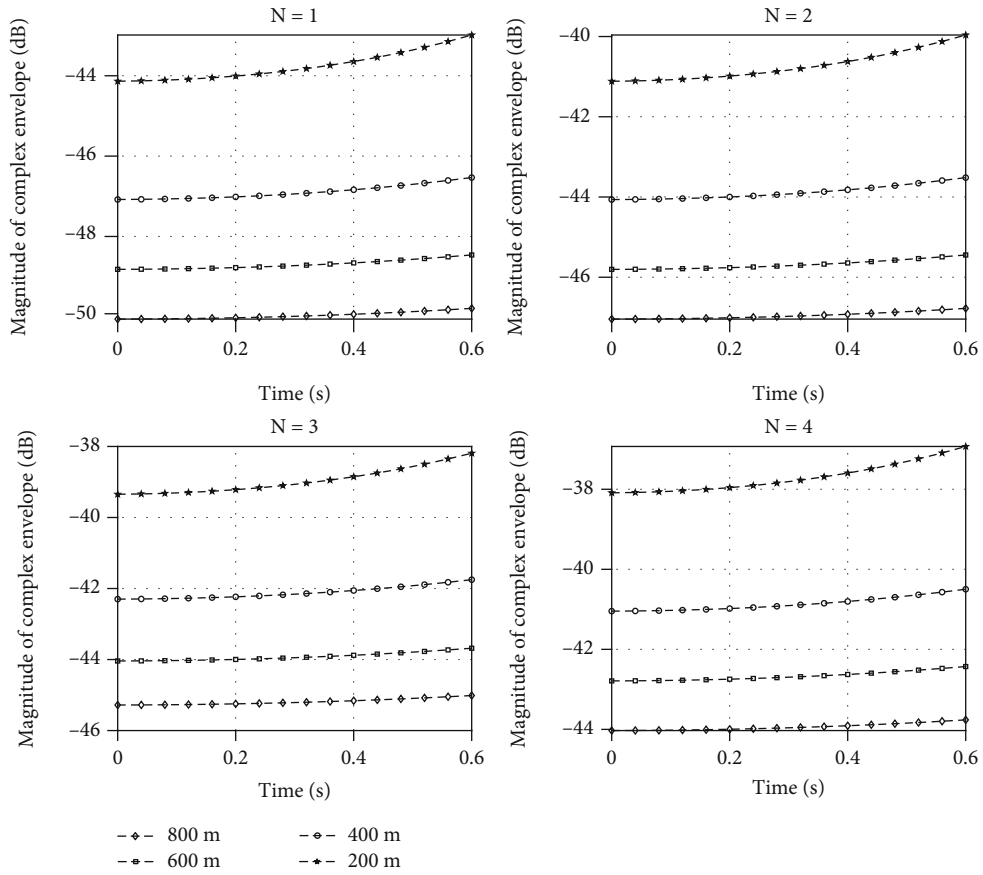

Figure 11: The magnitude of received signal in the presence of multiple reflectors when vehicle S moves from different distances for Equation (22).

increases by about 1.6% for $N = 1$ by comparing Figures 8 to 5. When $N = 4$, this result increases by about 2.5%. Similarly, we can observe the gain reaches to about from 1% to 3.6% when the initial distance is 800 m for vehicle S.

When the phase φ is 0 by controlling RISs, the magnitude of received signal in vehicle D is obtained from the Equation (22). With multiple RISs, the magnitude of the received signal on vehicle D is plotted in Figure 10 for different initial distances of vehicle S. From the initial distance change from 800 m to 200 m, the magnitude of the received signal on vehicle D is enhanced in multiple RISs-assisted systems. This ascribes the path loss to sudden decreases in signal transmission. Furthermore, the corresponding magnitude of the received signal at vehicle D is also displayed in Figure 11 when vehicle S moves from different initial distances. With increasing number of RISs, the magnitude of the received signal is enhanced in Figure 11 due to signals combined from multiple RISs-assisted links. Meanwhile, the smaller initial distance of vehicle S, the bigger magnitude of the received signal on vehicle D.

6. Conclusions and Future Work

In this paper, we have discussed the multipath fading and Doppler effect of mobile communications. Specifically, the signal is analyzed on the received terminal when the multiple reflectors are deployed in designed propagation scenarios. Then, we provided several methods by utilizing the RISs in eliminating and mitigating multipath fading and Doppler effect. The specific analysis models with reflectors-/RISs-assisted communication are proposed in this paper. Furthermore, the specific analysis on the received signal is given out in multiple RISs-assisted wireless communication systems when the LOS signal is blocked. All solutions on eliminating and mitigation multipath fading and Doppler effect are verified in simulations, and the performance of networks is improved in RISs-assisted mobile wireless communication systems.

All communication terminal are assumed to be in the same horizontal position in a two-dimensional (2D) environment in this paper. Without loss generality, the methods are suitable for a three-dimensional (3D) environment in mobile wireless networks. In future work, we will further analyze multipath fading and Doppler effect in RISs-assisted communication paradigm. The communication mechanism and data information processing are focused in the 3D environment. Furthermore, the deployment cost and system complexity should be caused attention to researchers for actual engineering application scenarios that require massive deployment of RISs.

Data Availability

The input data used to support the results of this research are included within the article.

Conflicts of Interest

The authors declare no conflict of interest. Guilu Wu's current address is School of Internet of Things Engineering, Jiangnan University, Wuxi, China.

Acknowledgments

This work was supported in part by the Jiangsu Planned Projects for Postdoctoral Research Funds project under Grant 2020Z113; in part by the National Mobile Communications Research Laboratory, Southeast University, under Grant 2020D17; in part by the Fundamental Research Funds for the Central Universities, under Grant JUSRP12020; in part by the National Natural Science Foundation of China, under Grant 61801227; in part by the Key Laboratory of Industrial Internet of Things & Networked Control, Ministry of Education of the People's Republic of China, under Grant 2019FF09; in part by the Qinglan Project of Jiangsu Province under Grant QLGC2021; and in part by the Future Network Scientific Research Fund Project under Grant FNSRFP-2021-YB-28.

References

[1] A. Morgado, K. Huq, S. Mumtaz, and J. Rodriguez, "A survey of 5G technologies: regulatory, standardization and industrial perspectives," *Digital Communications and Networks*, vol. 4, no. 2, pp. 87–97, 2018.

[2] W. Saad, M. Bennis, and M. Chen, "A vision of 6G wireless systems: applications, trends, technologies, and open research problems," *IEEE Network*, vol. 34, no. 3, pp. 134–142, 2020.

[3] Y. Wu, A. Khisti, C. Xiao, G. Caire, K. K. Wong, and X. Gao, "A survey of physical layer security techniques for 5G wireless networks and challenges ahead," *IEEE Journal on Selected Areas in Communications*, vol. 36, no. 4, pp. 679–695, 2018.

[4] E. Basar, M. di Renzo, J. de Rosny, M. Debbah, M. S. Alouini, and R. Zhang, "Wireless communications through reconfigurable intelligent surfaces," *IEEE Access*, vol. 7, pp. 116753–116773, 2019.

[5] P. Tang, R. Wang, A. F. Molisch, C. Huang, and J. Zhang, "Path loss analysis and modeling for vehicle-to-vehicle communications in convoys in safety-related scenarios," in *2019 IEEE 2nd Connected and Automated Vehicles Symposium (CAVS)*, pp. 1–6, Honolulu, HI, USA, 2019.

[6] G. Wu and H. Chu, "Spectrum sharing with vehicular communication in cognitive small-cell networks," *International Journal of Antennas and Propagation*, vol. 2020, Article ID 6897646, 10 pages, 2020.

[7] G. Wu, Z. Li, and H. Jiang, "Quality of experience-driven resource allocation in vehicular cloud long-term evolution networks," *Transactions on Emerging Telecommunications Technologies*, vol. 31, no. 8, article e4036, 2020.

[8] J. Zhao, "A survey of intelligent reflecting surfaces(IRSs): towards 6G wireless communication networks," 2019, https://arxiv.org/abs/1907.04789.

[9] A. K. Khandani, "Media-based modulation: a new approach to wireless transmission," in *2013 IEEE International Symposium on Information Theory*, pp. 3050–3054, Istanbul, Turkey, 2013.

[10] Y. Ding, K. J. Kim, T. Koike-Akino, M. Pajovic, P. Wang, and P. Orlik, "Spatial scattering modulation for uplink millimeter-wave systems," *IEEE Communications Letters*, vol. 21, no. 7, pp. 1493–1496, 2017.

[11] N. Kaina, M. Dupré, G. Lerosey, and M. Fink, "Shaping complex microwave fields in reverberating media with binary tunable metasurfaces," *Scientific Reports*, vol. 4, no. 1, 2014.

[12] L. Subrt and P. Pechac, "Intelligent walls as autonomous parts of smart indoor environments," *IET Communications*, vol. 6, no. 8, pp. 1004–1010, 2012.

[13] H. Yang, X. Cao, F. Yang et al., "A programmable metasurface with dynamic polarization, scattering and focusing control," *Scientific Reports*, vol. 6, no. 1, p. 35692, 2016.

[14] X. Tan, Z. Sun, D. Koutsonikolas, and J. M. Jornet, "Enabling indoor mobile millimeter-wave networks based on smart reflect-arrays," in *IEEE INFOCOM 2018 - IEEE Conference on Computer Communications*, pp. 270–278, Honolulu, HI, USA, 2018.

[15] F. Liu, O. Tsilipakos, A. Pitilakis et al., "Intelligent metasurfaces with continuously tunable local surface impedance for multiple reconfigurable functions," *Physical Review Applied*, vol. 11, no. 4, p. 044024, 2019.

[16] C. Huang, A. Zappone, M. Debbah, and C. Yuen, "Achievable rate maximization by passive intelligent mirrors," in *2018 IEEE International Conference on Acoustics, Speech and Signal Processing (ICASSP)*, pp. 3714–3718, Calgary, AB, Canada, 2018.

[17] C. Huang, A. Zappone, G. C. Alexandropoulos, M. Debbah, and C. Yuen, "Reconfigurable intelligent surfaces for energy efficiency in wireless communication," *IEEE Transactions on Wireless Communications*, vol. 18, no. 8, pp. 4157–4170, 2019.

[18] X. Qian, M. di Renzo, J. Liu, A. Kammoun, and M. S. Alouini, "Beamforming through reconfigurable intelligent surfaces in single-user MIMO systems: SNR distribution and scaling Laws in the presence of channel fading and phase noise," *IEEE Wireless Communications Letters*, vol. 10, no. 1, pp. 77–81, 2021.

[19] Q. Wu and R. Zhang, "Intelligent reflecting surface enhanced wireless network via joint active and passive beamforming," *IEEE Transactions on Wireless Communications*, vol. 18, no. 11, pp. 5394–5409, 2019.

[20] L. Yang, Y. Yang, M. O. Hasna, and M. S. Alouini, "Coverage, probability of SNR gain, and DOR analysis of RIS-aided communication systems," *IEEE Wireless Communications Letters*, vol. 9, no. 8, pp. 1268–1272, 2020.

[21] B. Zheng, C. You, and R. Zhang, "Intelligent reflecting surface assisted multi-user OFDMA: channel estimation and training design," *IEEE Transactions on Wireless Communications*, vol. 19, no. 12, pp. 8315–8329, 2020.

[22] G. T. de Araujo, A. L. F. de Almeida, and R. Boyer, "Channel estimation for intelligent reflecting surface assisted MIMO systems: a tensor modeling approach," *IEEE Journal of Selected Topics in Signal Processing*, vol. 15, no. 3, pp. 789–802, 2021.

[23] P. Wang, J. Fang, H. Duan, and H. Li, "Compressed channel estimation for intelligent reflecting surface-assisted millimeter wave systems," *IEEE Signal Processing Letters*, vol. 27, pp. 905–909, 2020.

[24] X. Chen, J. Shi, Z. Yang, and L. Wu, "Low-complexity channel estimation for intelligent reflecting surface-enhanced massive MIMO," *IEEE Wireless Communications Letters*, vol. 10, no. 5, pp. 996–1000, 2021.

[25] S. Xu, J. Liu, and Y. Cao, "Intelligent reflecting surface empowered physical layer security: signal cancellation or jamming?," *IEEE Internet of Things Journal*, p. 1, 2021.

[26] K. Feng, X. Li, Y. Han, S. Jin, and Y. Chen, "Physical layer security enhancement exploiting intelligent reflecting surface," *IEEE Communications Letters*, vol. 25, no. 3, pp. 734–738, 2021.

[27] X. Lu, J. Lei, Y. Shi, and W. Li, "Intelligent reflecting surface assisted secret key generation," *IEEE Signal Processing Letters*, vol. 28, pp. 1036–1040, 2021.

[28] S. Abeywickrama, R. Zhang, Q. Wu, and C. Yuen, "Intelligent reflecting surface: practical phase shift model and beamforming optimization," *IEEE Transactions on Communications*, vol. 68, no. 9, pp. 5849–5863, 2020.

[29] M. Fu, Y. Zhou, and Y. Shi, *Intelligent Reflecting Surface for Downlink Non-Orthogonal Multiple Access Networks*, IEEE Globecom workshops (GC Wkshps), Waikoloa, HI, USA, 2019.

[30] Z. Ding and P. H. Vincent, "A simple design of IRS-NOMA transmission," *IEEE Communications Letters*, vol. 24, no. 5, pp. 1119–1123, 2020.

[31] F. P. Fontan and P. M. Espineira, *Modeling the Wireless Propagation Channel: A Simulation Approach with MATLAB*, Wiley, United Kingdom, 2008.

[32] E. Basar and I. F. Akyildiz, "Reconfigurable intelligent surfaces for Doppler effect and multipath fading mitigation," 2019, http://arxiv.org/abs/1912.04080v1.